Comparison between the fragmentation processes in central Pb + Ag and Pb + Au collisions

Benoit Jouault, Guy Royer, J.F. Lecolley, Fayrouz. Haddad, F. Sebille

ECOLE DES MINES DE NANTES

SUBATECH

UMR Université, Ecole des Mines, IN2P3/CNRS

LABORATOIRE DE PHYSIQUE SUBATOMIQUE
ET DES TECHNOLOGIES ASSOCIEES

COMPARISON BETWEEN THE FRAGMENTATION PROCESSES IN CENTRAL Pb + Ag AND Pb + Au COLLISIONS

B. Jouault, G. Royer, J.F. Lecolley, F. Sébille and F. Haddad

Rapport Interne SUBATECH 96-06

4, RUE ALFRED KASTLER. LA CHANTRERIE. 44070 NANTES CEDEX 03. TELEPHONE 51 85 81 00. TELECOPIE 51 85 84 79. E-mail : @ FRCPN11.IN2P3.FR

Comparison between the fragmentation processes in central Pb + Ag and Pb + Au collisions

B. Jouault[a], G. Royer[a], J.F. Lecolley[b], F. Sebille[a] and F. Haddad[a]
[a]Laboratoire de Physique Subatomique et des Technologies Associées,
UMR : IN2P3/CNRS, Université et Ecole des Mines de Nantes,
2 rue de la Houssinière, 44072 Nantes Cedex 03, France
[b]Laboratoire de Physique Corpusculaire Caen (IN2P3-CNRS/ISMRA et Université de Caen), bld Maréchal Juin, 14050 Caen Cédex, France

Abstract :
The fragmentation processes of a medium mass system and of a very massive one formed in central collisions are compared within the Landau-Vlasov model taking into account both the isospin dependence and the two-body residual interactions. The simulations predict the formation of a roughly ellipsoidal source in the central Pb + Ag reactions while, for the Pb + Au system, the fragmentation occurs from an hollow source, the configuration of which being intermediate between bubble-like and toroidal shapes. This different shapes explain and allow to reproduce semi-quantitatively the two different profiles of the experimental kinetic energy spectra.

1. Introduction

The complete study of hot and compressed or dilute nuclear matter is now possible with the advent of heavy-ion accelerators delivering projectile energy up to 100 MeV/u and of very efficient 4π detectors [1]. Available data have proved the persistence at these energies of the fusion, fission and deep-inelastic regimes and the emergence of new processes like multifragment disintegration, vaporization and strong evaporation [2-5]. It is quite difficult from the detection of several intermediate mass fragments to trace the fragmentation process back to its origin. Furthermore, statistical fragmentation models [6-8] are sufficient to explain the branching ratios of the different channels [9] and most of the experimental data [10]. Nevertheless, before the decay, a large portion of the mass, energy and angular momentum is radiated which significantly reduces the fragmentation width [11] and it is important to know to what extent the dynamic plays a role. For example, it has been shown that with increasing beam energy the type of disintegration of the Ar + Au system evolves from sequential breakup of excited fragments to almost simultaneous explosion of a very hot system [12]. In peripheral collisions, the intermediate mass fragment production mechanism is mainly the multiple neck rupture [13-14].

Central collisions between heavy nuclei are of particular relevance to generate the fragmentation process at relatively low intermediate energies since the thermodynamic limit is more readily reached and since these reactions cannot lead to stable compound nuclei. Recently, the Pb(29 MeV/u) + Au and Au(35 MeV/u) + Au reactions have been investigated and multifragment disintegrations have effectively been observed [2,5,10,15]. Experimental evidence for the formation of toroidal structures in very central Pb(29 MeV/u) + Au collisions has been advanced [16-17]. More than 20 years ago, Wong [18] predicted, within the liquid drop model, that due to the competition between Coulomb and surface effects exotic shapes like toroids might be metastable but only for very heavy systems. New macroscopic calculations [19-20] taking into account both the proximity effects and the temperature in the estimation of the potential energies have led to similar conclusions. Recently, simulations based on microscopic approaches [21-24], temperature time-dependent Hartree-Fock model [25] and hydrodynamical calculations [26] have also predicted the formation of exotic configurations like disks, toroids and bubbles just after the most violent phase of central heavy-ion collisions and prior to fragmentation.

The purpose of the present work is to study the fragmentation process in central Pb + Ag reactions at 29 MeV/u within the microscopic semi-classical Landau-Vlasov model and to compare with experimental data and also with the theoretical and experimental results obtained for the Pb(29 MeV/u) + Au collisions. The aim is to know whether metastable hollow sources are also predicted and observed in central Pb + Ag reactions and, then, the dependence of the multifragmenting source topology on the mass of the total system. In Section 2, the model is briefly reviewed. The results of the simulations of the Pb + Ag reaction are given and analysed in section 3. They are compared in Section 4 to the predictions relative to the Pb + Au reaction. In Section 5, the simulations for the two reactions are compared with experimental data. Finally, the dependence of the fragmentation process on the projectile energy is studied in Section 6.

2. Semi-classical microscopic model

The Landau-Vlasov model describes the dynamics of nuclear collisions through a phase-space transport equation complemented by a Pauli-blocked Uehling-

Uhlenbeck collision term I_{coll}. Such an approach allows to remove the shape constraints. The reliability of this method to describe long time processes such as hot fission and deep-inelastic collisions [27] as well as the equation of state of nuclear matter for many different interactions with zero or finite range [28] and the violent decay of an isolated rotating nucleus [29] has previously been demonstrated.

In this model [30], the time evolution of the one-body phase-space distribution function $f(\vec{r}, \vec{p}; t)$ is driven by the kinetic equation :

$$\frac{\partial f}{\partial t} + \{f, H\} = I_{coll}(f), \tag{1}$$

where { } stands for the Poisson bracket and H is the one-body Hamiltonian describing the mean field taken as only density dependent. The free isospin and energy dependent nucleon-nucleon cross section has been selected.

This equation is solved by projecting $f(\vec{r}, \vec{p})$ onto a moving basis of coherent states which are frozen-width gaussians,g , in coordinate and momentum spaces :

$$f(\vec{r}, \vec{p}) = \frac{A}{N_g} \sum_i \omega_i g_\chi(\vec{r} - \vec{r}_i)\, g_\phi(\vec{p} - \vec{p}_i). \tag{2}$$

N_g is the number of coherent states, ω_i weight factors determined by the initial conditions and χ and ϕ the respective variances. The local density follows :

$$\rho(\vec{r}) = \int f(\vec{r}, \vec{p}) d^3\vec{p}. \tag{3}$$

The mean field is described by a simplified version of the zero-range Skyrme effective force, the Zamick interaction, with an extra isospin dependent term :

$$U_q(\rho, \xi) = t_0 \frac{\rho}{\rho_0} + t_3 (\frac{\rho}{\rho_0})^{1+\nu} + c \frac{\xi^2}{\rho_0^2} + 4 \frac{cq\rho\xi}{\rho_0^2}, \tag{4}$$

with $\rho = \rho_n + \rho_p$ and $\xi = \rho_n - \rho_p$. (5)

ρ_n (ρ_p) is the neutron (proton) local density and q = 0.5 (-0.5) for neutrons (protons). The parameter values are

t_0 = -356 MeV, t_3 = 303 MeV, ν = 1/6 and c = 20 MeV. (6)

The local collective velocity field in the center of mass frame reads :

$$\vec{V}_{coll}(\vec{r}) = \frac{1}{m\rho(\vec{r})} \int \vec{p} f(\vec{r}, \vec{p}) d^3\vec{p}. \tag{7}$$

It follows the collective kinetic energy :

$$E_{coll} = \frac{1}{2} m \int \rho(\vec{r}) V_{coll}^2(\vec{r}) d^3\vec{r}. \tag{8}$$

The surface energy can be evaluated by :

$$E_{surf} = \frac{a_s}{4\pi r_0^2} \frac{A}{\langle\rho\rangle} \frac{\int \rho(\vec{r}) \left| grad(\rho(\vec{r})) \right| d^3\vec{r}}{\int \rho(\vec{r})^2 d^3\vec{r}}. \tag{9}$$

3. From peripheral to central collisions in the Pb(29 MeV/u) + Ag reaction

Before to focus on central collisions, it is important to have a global overview of the reaction and to examine the predictions of the model in the whole impact parameter range.

To display the experimental total kinetic energy of the fragments as a function of the angular distribution, the Wilczynski diagrams have been generalized [2] defining the following tensor :

$$F_{ij} = \sum_{n=1}^{M_f} \frac{1}{2m_n} P_i^{(n)} P_j^{(n)} \quad (i, j = 1, 2, 3), \tag{10}$$

$P_k^{(n)}$ being the kth Cartesian coordinate of the momentum $P^{(n)}$ of the nth fragment with mass m_n. In this picture, the angle θ_{cm} is defined as the angle between the beam axis and the flow direction defined by the eigenvector associated to the largest eigenvalue. In figure 1, the contour plots indicate the experimental data. They have the usual distribution. For peripheral collisions, there is almost no deviation and no loss of kinetic energy. With decreasing impact parameters, the energy dissipation increases which slackens the outgoing fragments. For the most central collisions, there is a saturation of the dissipated energy and the deviation angle covers the whole angular possibilities. It is beyond the scope of our approach to address the problem of the fluctuations around the mean values but, at least, the present model agrees correctly with the general trends of the experimental data.

A measure of the memory of the entrance channel distribution of matter is plotted in figure 2, in order to study the limit of the deep-inelastic regime and the nature of the multifragmentating sources. This memory may be evaluated as the mean absolute difference between the ratios of the number of nucleons originating from the projectile (resp target) in one fragment to the total number of nucleons coming from the projectile (resp target) in all fragments.

$$n_{mem} = \left\langle \left| \frac{n_{p_i}}{\sum_i n_{p_i}} - \frac{n_{t_i}}{\sum_i n_{t_i}} \right| \right\rangle_{i=1,2,\ldots n.} \tag{11}$$

The memory diminishes with decreasing impact parameters and vanishes for $b \leq 4$ fm. Then, around 4 fm a transition occurs from deep-inelastic collisions to formation of an unique hot evanescent multifragmenting source which has lost the memory of the initial constituents of the reaction but, naturally, not of the available energy and angular momentum due to conservation laws.

To analyse the spatial distribution of nucleons during the reactions, the tensor $t_{ij} = \sum_{l=1}^{N_g} x_i^{(l)} x_j^{(l)}$ has been diagonalized and the evolution of the square root of the eigenvalues λ_i is displayed in figure 3. Such pictures do not allow to know precisely what happens when all the nucleons are very close to each other in the first phase of the reaction but they can give a first idea of the source when one looks at the asymptotic behaviour. At b= 0 fm, the nucleons remain together on two directions and move from each other on a preferred axis. This corresponds to the emission of two fragments. The system having lost memory of the entrance channel, this event looks like a binary hot fission process. At b = 2 fm, the same type of reaction takes place but more rapidly. At b = 4 fm, the distribution of matter spreads in two directions (given by the dotted and dashed curves) indicating the existence of several fragments. The difference between the expansion velocities are due to the memory of the initial

direction of the beam. The products of the collision are mainly emitted in a plane since the third component (full curve) does not evolve and, then, the source has rather a disk or toroid shape. At b = 6 fm the emission is also bi-dimensional but much more rapid and some memory of the entrance channel is conserved. This reaction is of deep-inelastic type and leads to multifragmentation. Finally the peripheral reaction at b = 8 fm leads to the formation of an elongated shape with a neck and, later on, to the emission of two main fragments and of a light one reminiscent of the neck matter.

4. Comparison between the Pb + Ag and Pb + Au reactions at 29 MeV/u

The Pb + Au reaction has been recently investigated both experimentally and theoretically [2,16-17,23]. It leads to one of the heaviest studied systems allowing to maximize the Coulomb repulsion and neutron-proton asymmetry effects. In central collisions, after the strong compression in the overlap region, the whole nuclear mass becomes very compact. Later on, the system expands due to the saturation of the nuclear forces and Coulomb repulsion. In a third phase, a depletion appears in the heart of the matter distribution leading to the formation of a very distorted configuration intermediate between bubble and toroid. Finally, instabilities develop to minimize the surface tension and this hollow shape breaks up into several fragments. This multifragment disintegration of an hollow source does not occur if the Coulomb repulsion or the isospin or the two-body collisions are disconnected in the simulation [23].

The evolution of the density profiles in the central Pb(29 MeV/u) + Ag reaction are displayed in figures 4 and 5. After the compression and expansion phases, a hole begins to appear at the center of the nuclear mass but it is progressively filled up and the fragmenting source at around 400 fm/c is relatively equilibrated. Later on, this source follows the hot binary fission channel at b = 0 fm.

The differences between the exit channels in the Pb + Ag and Pb + Au reactions at b = 2 fm are also illustrated in figures 6 and 7. Already, during the expansion phase corresponding to an hump in the diagrams, two components increase more rapidly than the third one in the Pb + Au reaction but not in the Pb + Ag reaction. This is another signature of the formation of an hollow configuration in the Pb + Au collision. Later on, the hollow source breaks up in several fragments emitted preferentially in a plane or, at least, in a small solid angle. In the Pb + Ag reaction, the two fragments progressively go away from each other.

The two phases of compression and expansion appear respectively at around 80 fm/c and 170 fm/c and correspond respectively naturally at a maximum and a minimum of the Coulomb repulsion and a minimum and maximum of the surface energy. After, the profiles are no more the same. The surface does not decrease so strongly in the Pb + Au reaction since the hole in the matter contributes also to the surface energy and since the greatest number of fragments increases also the surface energy relatively to the binary exit channel. The differences are less important for the Coulomb energy but, nevertheless, a small hump is visible in the case of the Pb + Ag reaction and not in the case of the Pb + Au reaction since the matter is already more spread.

5 Comparison with experimental data

Experimentally (figure 8) the velocity of the fragments decreases strongly with the charge in the Pb + Ag reaction and very weakly in the Pb + Au reaction. As a result and on account of the linear dependence on the charge and the square of the

velocity, the kinetic energy increases regularly with the charge in the Pb + Au collisions while the kinetic energy spectrum presents a maximum for intermediate charges in the Pb + Ag reaction. The two velocity distributions allow to discriminate between the source shapes. For disks, the fragments are produced everywhere and the velocity distribution is broad. The heaviest fragments are formed in the center of the matter and have the lowest velocities at infinity. For toroids, fragments are more located near the surface and play roughly the same role and the velocity distribution is narrow. This confirms the predominance of disintegrating disk-like sources in central Pb + Ag collisions and of multifragmentation of toroidal sources in central Pb + Au collisions. The values obtained from different simulations reproduce the different shapes and profiles of the experimental spectra, even if the lack of statistics somewhat scatters the theoretical points.

6. Dependence of the fragmentation process on the projectile energy

The figure 9 gives a first idea of the evolution of the disassembly mode with energy. The $\sqrt{\lambda_i}$ scale has been adjusted in each panel. At 40 MeV/u, the simulation leads to a very distorted hollow source which breaks up in one heavy fragment and three lighter ones, the largest fragment decaying probably sequentially after a long time. It essentially comes from the external part of the Pb nucleus which has less interacted with the target. At 55 MeV/u, the reaction is so violent and, then so rapid, that the relaxation and mixing of the nucleons are less important and there is no more, really, formation of a semi-equilibrated source. The reaction rather looks like an explosion where the fragments are more distributed in the three dimensional space and have more conserved the memory of the entrance channel since there are mainly parts of the projectile or the target, the interaction time allowing not a full redistribution of the nucleons.

7. Conclusion

Calculations on the Pb + Ag reaction at 29 MeV/u have been reported and compared with experimental data and with results obtained in the study of the Pb(29 MeV/u) + Au collisions. The theoretical investigation has been performed within the semi-classical Landau-Vlasov model including a Uehling-Uhlenbeck collision term and a soft equation of state with an isospin dependence.

The predictions agree with the Wilczynski diagram. For central impact parameter values ($b \leq 4$ fm), the fully damped nuclear system has forgotten the memory of the entrance channel. For the most central collisions, the hot binary fission process takes place. For the intermediate central reactions, fragmentation from an ellipsoidal (disk) source occurs and the fragments are emitted in a small solid angle. The deep-inelastic regime leads also to the fragmentation process for the more peripheral collisions, putting forward the important role of the angular momentum. So, the formation of an hollow source intermediate between bubble and toroid predicted and observed in the central Pb + Au collisions is not predicted in the central Pb + Ag reactions. The difference between the shape of the sources in these two reactions is sufficient to explain the respective narrowness and broadness of the velocity distribution observed in the Pb + Au and Pb + Ag reactions.

REFERENCES

[1] F. Saint-Laurent, Nucl. Phys. A 583 (1995) 481c
[2] J.F. Lecolley et al, Phys. Lett. B 325 (1994) 317
[3] W.G. Lynch, Nucl. Phys. A 583 (1995) 471c
[4] C.O.Bacri et al, Phys. Lett. B 353 (1995) 27
[5] M. D'Agostino et al, Phys. Lett. B 368 (1996) 259
[6] J.P. Bondorf, R. Donangelo, I.N. Mishustin, C.J. Pethick, H. Schutz and K. Sneppen, Nucl. Phys. A 443 (1985) 231
[7] D.H.E Gross, Rep. Prog. Phys. 53 (1990) 605
[8] J.P. Bondorf, A.S. Botvina, A.S. Iljinov, I.N. Mishustin and K. Sneppen, Phys.Rep. 257 (1995) 133
[9] L.G. Moretto, D.N. Delis and G.J. Wozniak, Phys. Rev. Lett 71 (1993) 3935
[10] M. D'Agostino et al, Phys. Lett. B 371 (1996) 175
[11] J.A. Lopez and J. Randrup, Nucl. Phys. A 571 (1994) 379
[12] M. Louvel et al, Phys. Lett. B 320 (1994) 221
[13] J. Toke et al, Phys. Rev. Lett. 75 (1995) 2920
[14] B. Jouault, V. de la Mota, F. Sebille, G. Royer and J.F. Lecolley, Nucl. Phys. A 597 (1996) 136
[15] R.Bougault et al, Nucl. Phys. A 587 (1995) 499
[16] J.F. Lecolley et al, LPCC report 01 (1996), Phys. Lett. B (1996) submitted
[17] D. Durand et al, LPCC report 02 (1996), Phys. Lett. B (1996) submitted
[18] C.Y. Wong, Ann.of. Phys. 77 (1973) 279
[19] C. Fauchard and G. Royer, Nucl. Phys. A 598 (1996) 125
[20] G. Royer, F. Haddad and B. Jouault, Nucl. Phys. A (1996) in print
[21] W. Bauer, G.F. Bertsch and H. Schulz, Phys. Rev. Lett. 69 (1992) 1888
[22] S.R. Souza and C. Ngô, Phys.Rev.C 48 (1993) R2555
[23] B.Jouault, F. Sebille, G. Royer and V. de la Mota, Nucl. Phys. A 591 (1995) 497
[24] H.M.Xu, C.A. Gagliardi, R.E. Tribble and C.Y. Wong, Nucl. Phys. A 569 (1994) 575
[25] H.Ngô, F.Z. Ighezou, C.Ngô, J.Nemeth and L. Depaola, XXI Workshop on gross properties of nuclei and nuclear excitations, Hirschegg, Austria 1993 (GSI, Darmstadt, 1993) 302
[26] C.E. Aguiar, R. Donangelo, C.O. Dorso, R.S. Gomes and N. Gonçalves, Phys. Rev. C 46 (1992) 1069
[27] F.Haddad, G. Royer, F. Sebille and B. Remaud, Nucl. Phys. A 572 (1994) 459
[28] F. Sebille, G. Royer, C. Gregoire, B. Remaud and P. Schuck, Nucl. Phys. A 501 (1989) 137
[29] F. Garcias, V. de la Mota, B. Remaud, G. Royer and F. Sebille, Phys. Lett. B 255 (1991) 311
[30] C. Gregoire, B. Remaud, F. Sebille, L. Vinet and Y. Raffray, Nucl. Phys. A 465 (1987) 317

FIGURE CAPTIONS

Figure 1 : Comparison between the generalized Wilczynski diagram for a fragment multiplicity $M_f > 2$ and our theoretical results (indicated by dots) obtained from simulations at different impact parameters.

Figure 2 : Memory of the entrance channel in the outgoing fragments as a function of the impact parameter in the Pb (29 MeV/u) + Ag reaction.

Figure 3 : Time evolution of the three geometric components $\sqrt{\lambda_i}$ characterizing the spatial distribution of matter as a function of the impact parameter in the Pb (29 MeV/u) + Ag reaction.

Figure 4 : Time evolution of the nuclear densities at b = 0 fm in the Pb (29 MeV/u) + Ag reaction. The horizontal z axis indicates the beam direction. The time (fm/c unit) is given in the right upper corner of each panel.

Figure 5 : Time evolution of the density (in nucl/fm^3) in the Pb (29 MeV/u) + Ag reaction at b = 0 fm along the main axis of the matter distribution. The time indicated in each panel is in fm/c and the position in fm.

Figure 6 :Time evolution of the distribution of matter in the two reactions Pb + Ag and Pb + Au at b = 2 fm.

Figure 7 : Time evolution of the Coulomb and surface energies (in MeV) for the Pb + Ag and Pb + Au reactions at 29 MeV/u.

Figure 8 : Velocities and kinetic energies of the emitted fragments as a function of their atomic number Z for the Pb + Ag and Pb + Au reactions at 29 MeV/u. Dots indicate results of the simulations while bars correspond to experimental data.

Figure 9 : Time evolution of the matter distribution as a function of the beam energy for the Pb + Ag reaction at b = 2 fm.

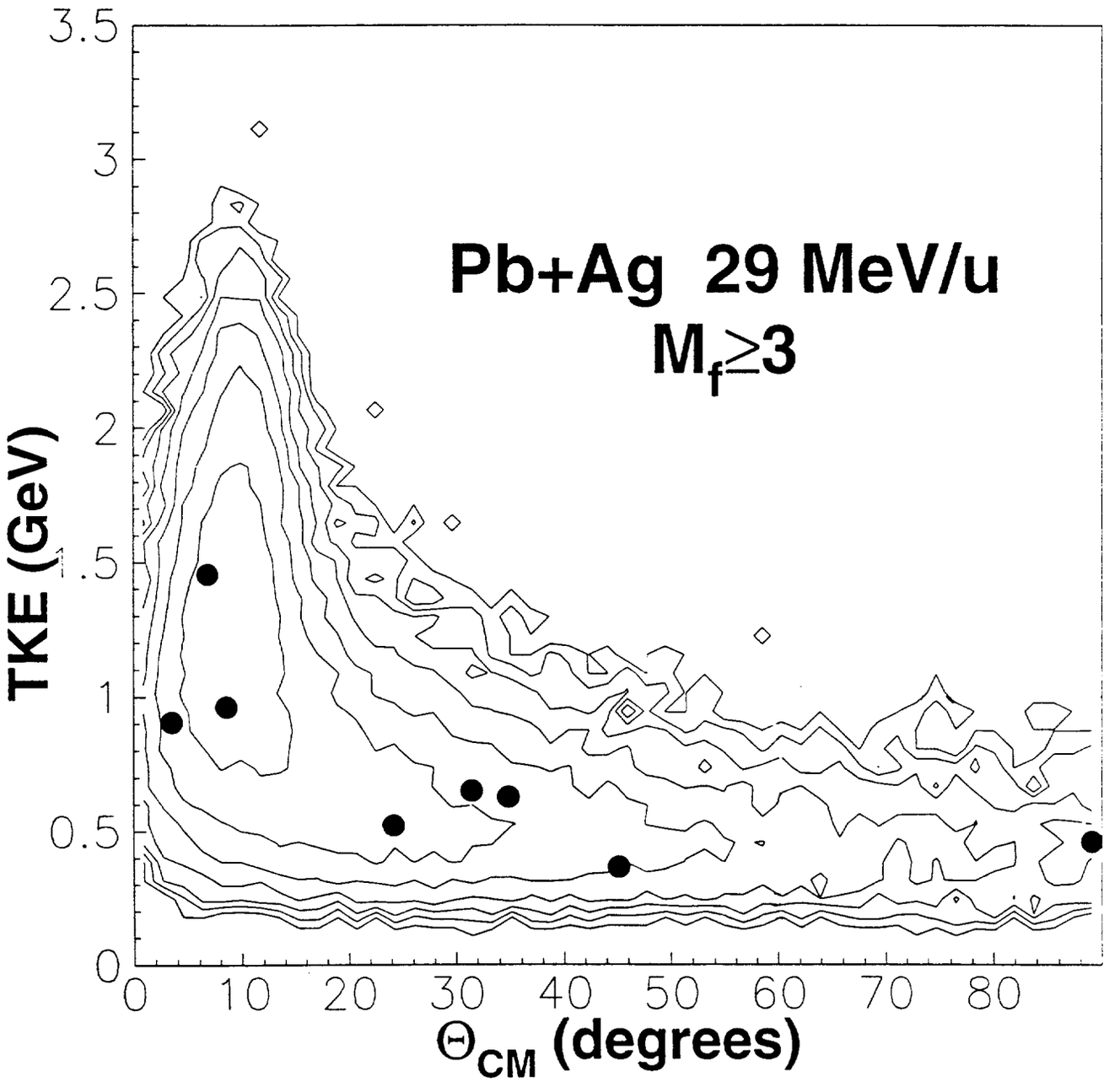
Pb+Ag 29 MeV/u
$M_f \geq 3$
TKE (GeV)
Θ_{CM} (degrees)
0
0.5
1
1.5
2
2.5
3
3.5
0
10
20
30
40
50
60
70
80

Figure 1

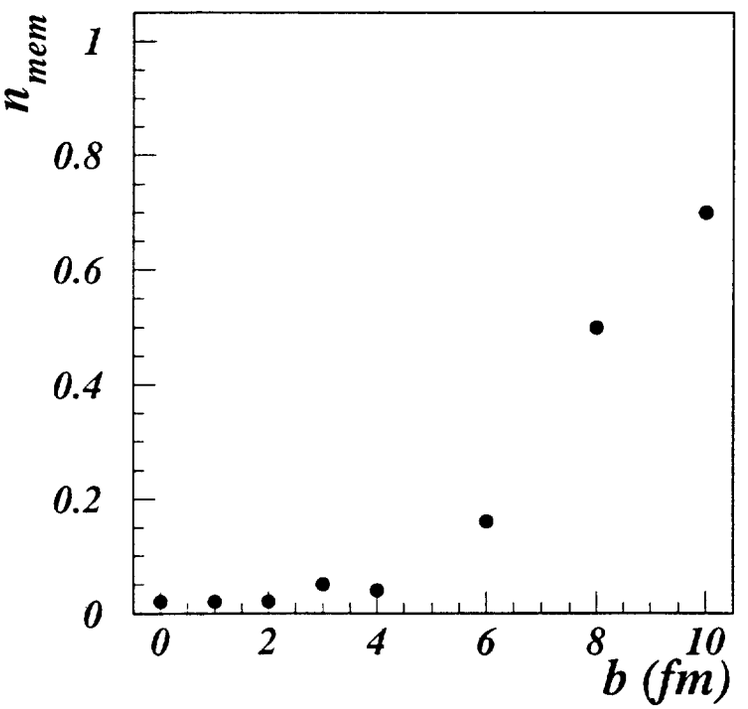

Figure 2

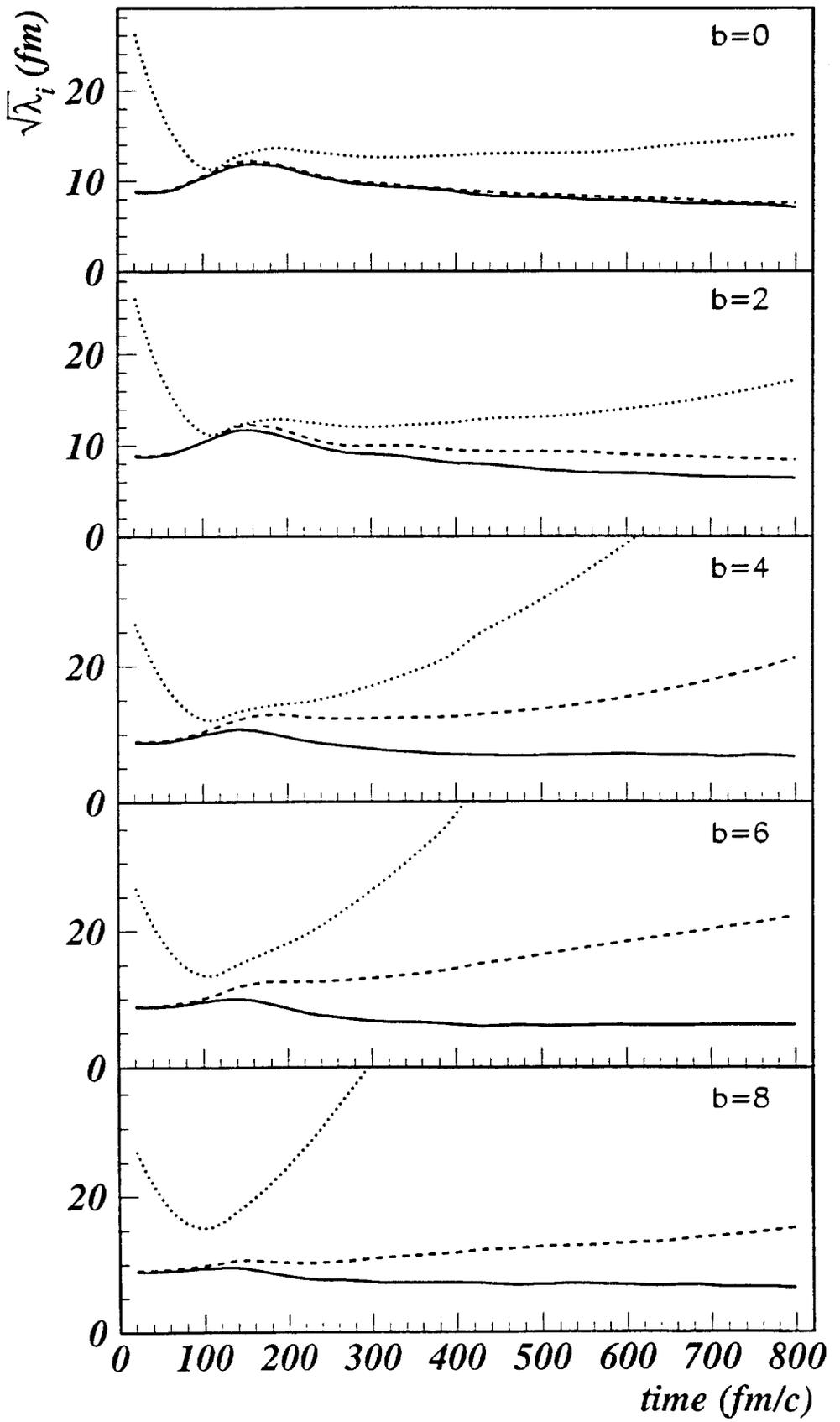
$\sqrt{\lambda_i}$ (fm)
b=0
b=2
b=4
b=6
b=8
0
10
20
0 100 200 300 400 500 600 700 800
time (fm/c)

Figure 3

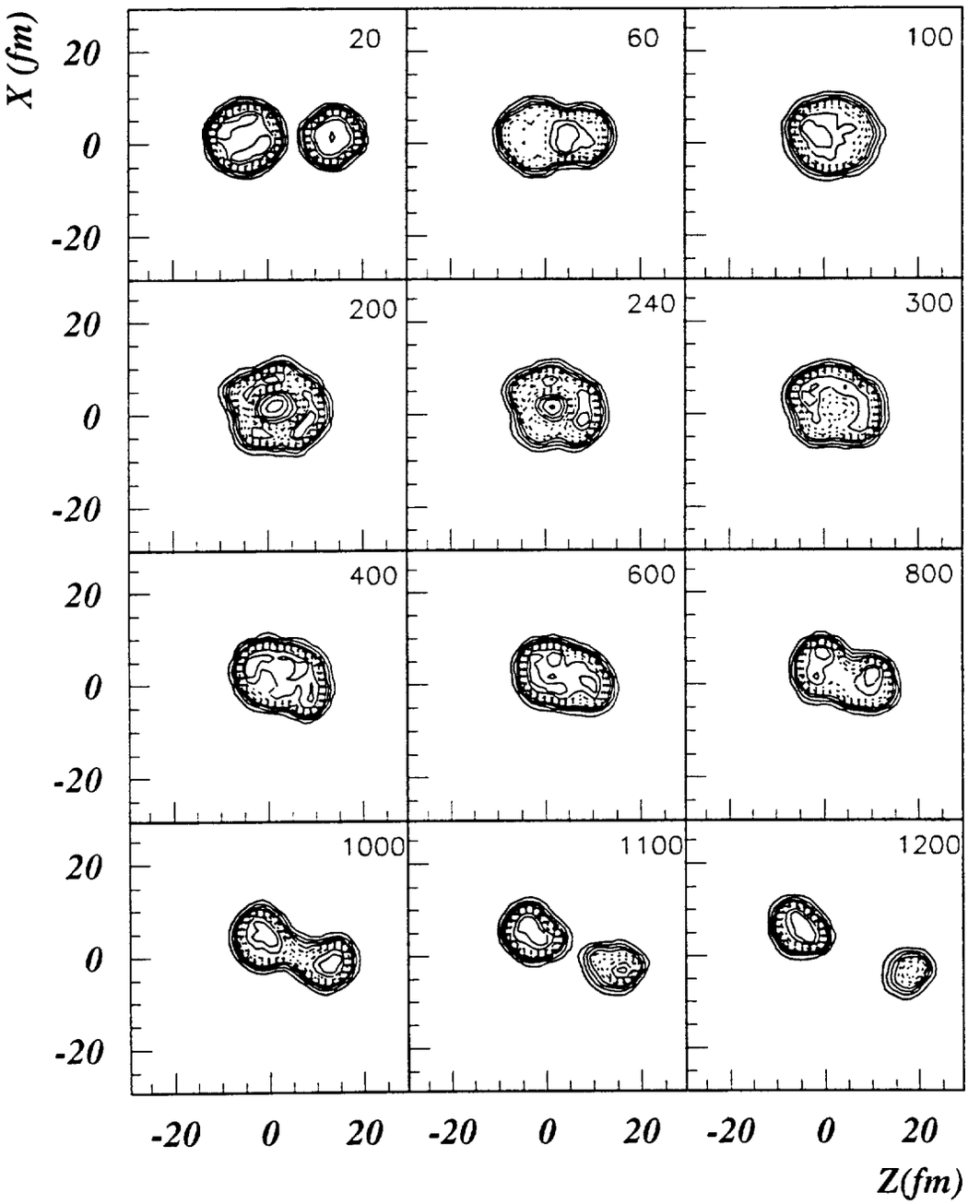
X (fm)
20
0
-20
20
60
100
200
240
300
400
600
800
1000
1100
1200
-20
0
20
Z(fm)

Figure 4

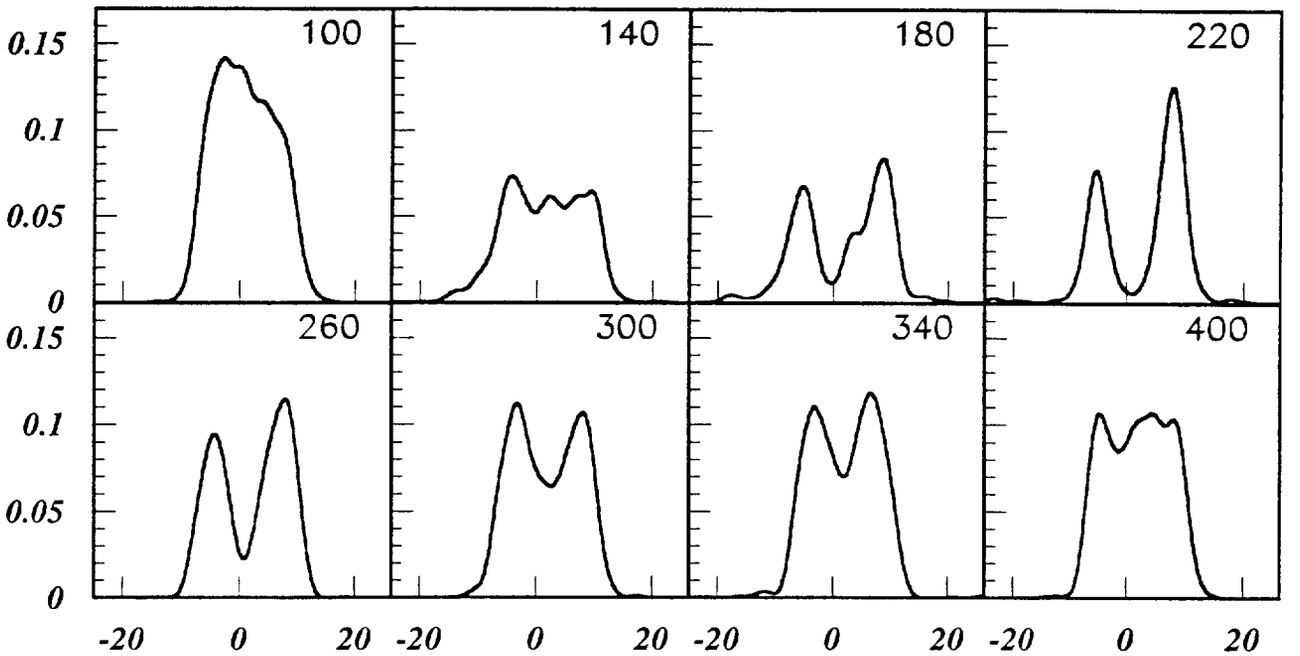

Figure 5

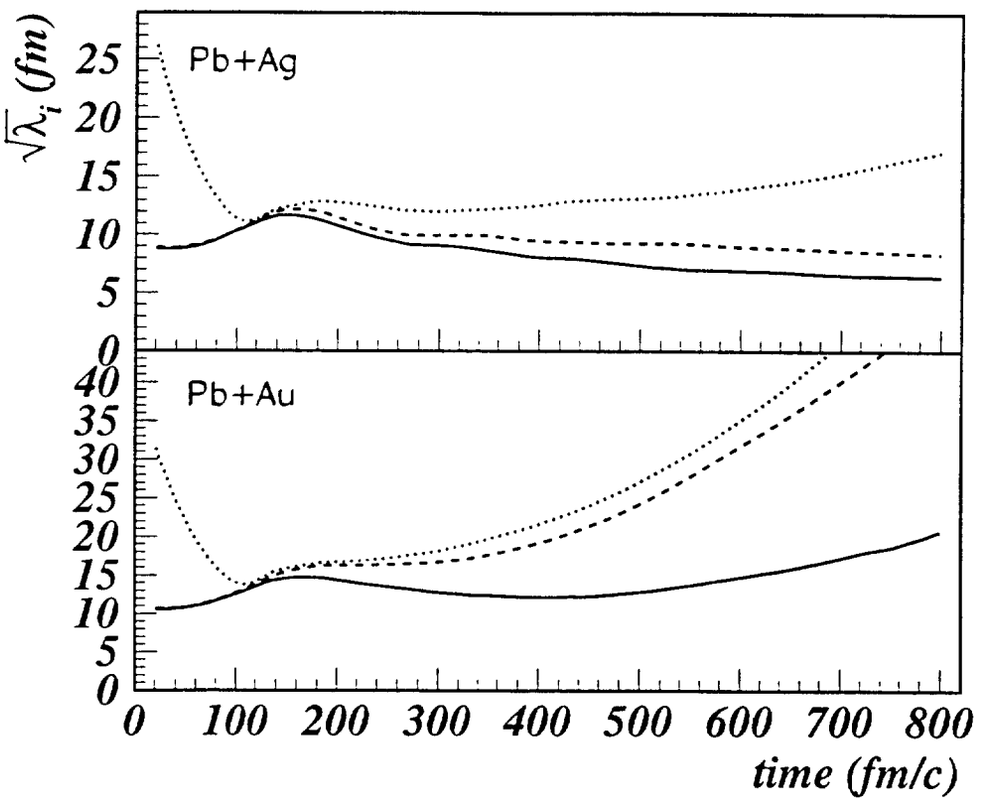
$\sqrt{\lambda_i}$ (fm)
Pb+Ag
25
20
15
10
5
0
Pb+Au
40
35
30
25
20
15
10
5
0
0
100
200
300
400
500
600
700
800
time (fm/c)

Figure 6

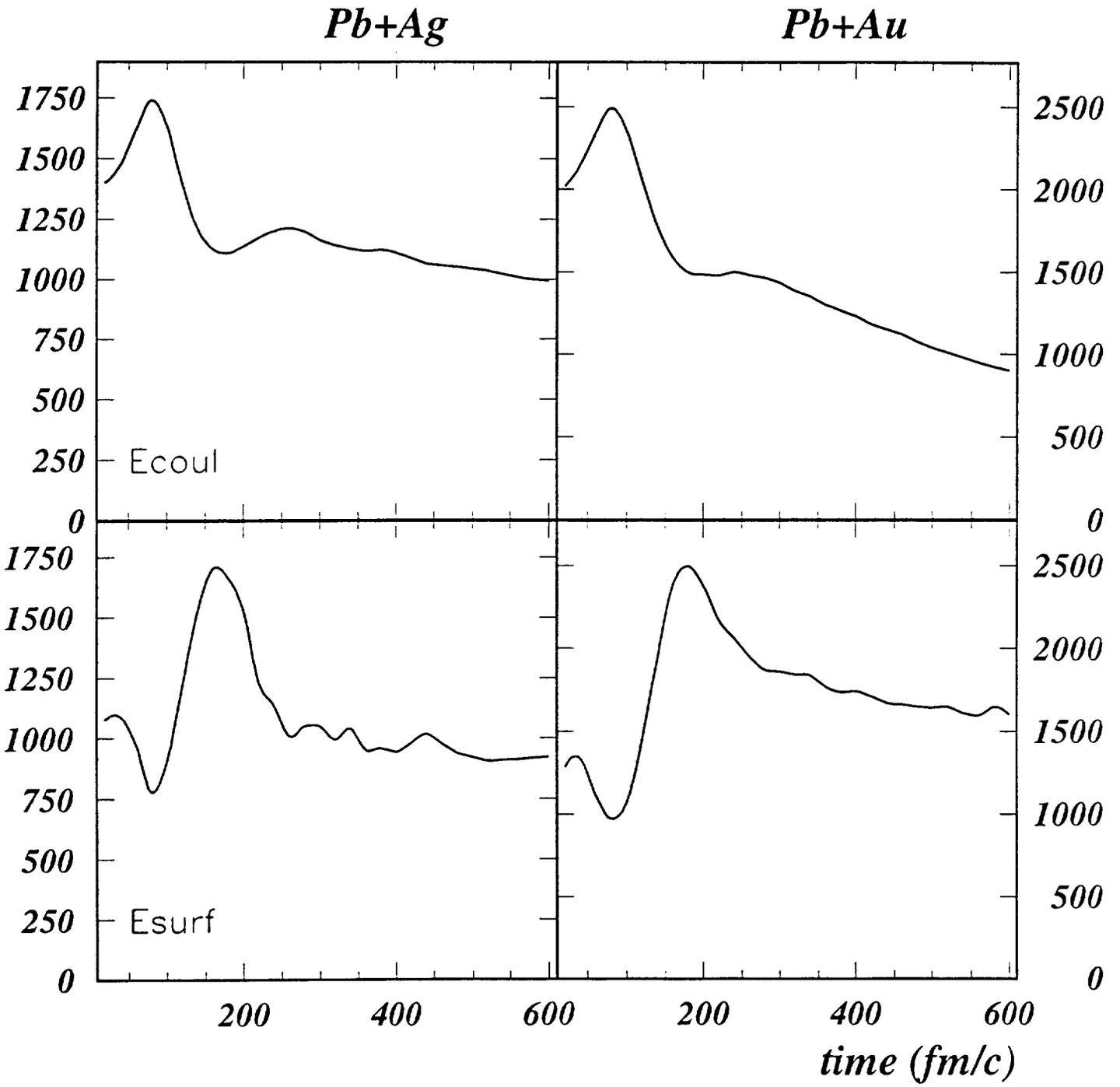
Pb+Ag
Pb+Au
1750
1500
1250
1000
750
500
250
0
Ecoul
2500
2000
1500
1000
500
0
Esurf
200
400
600
time (fm/c)

Figure 7

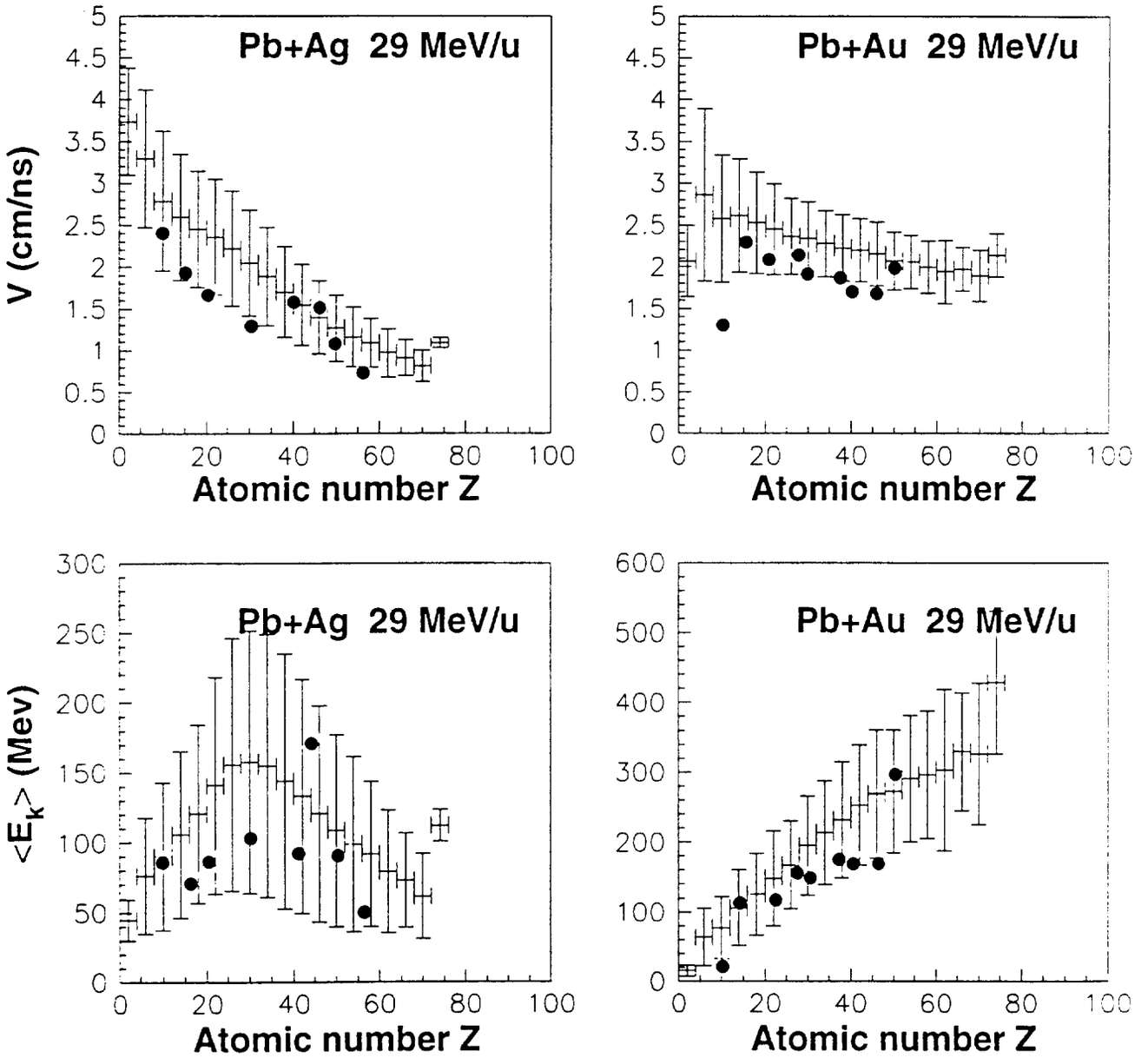

Figure 8

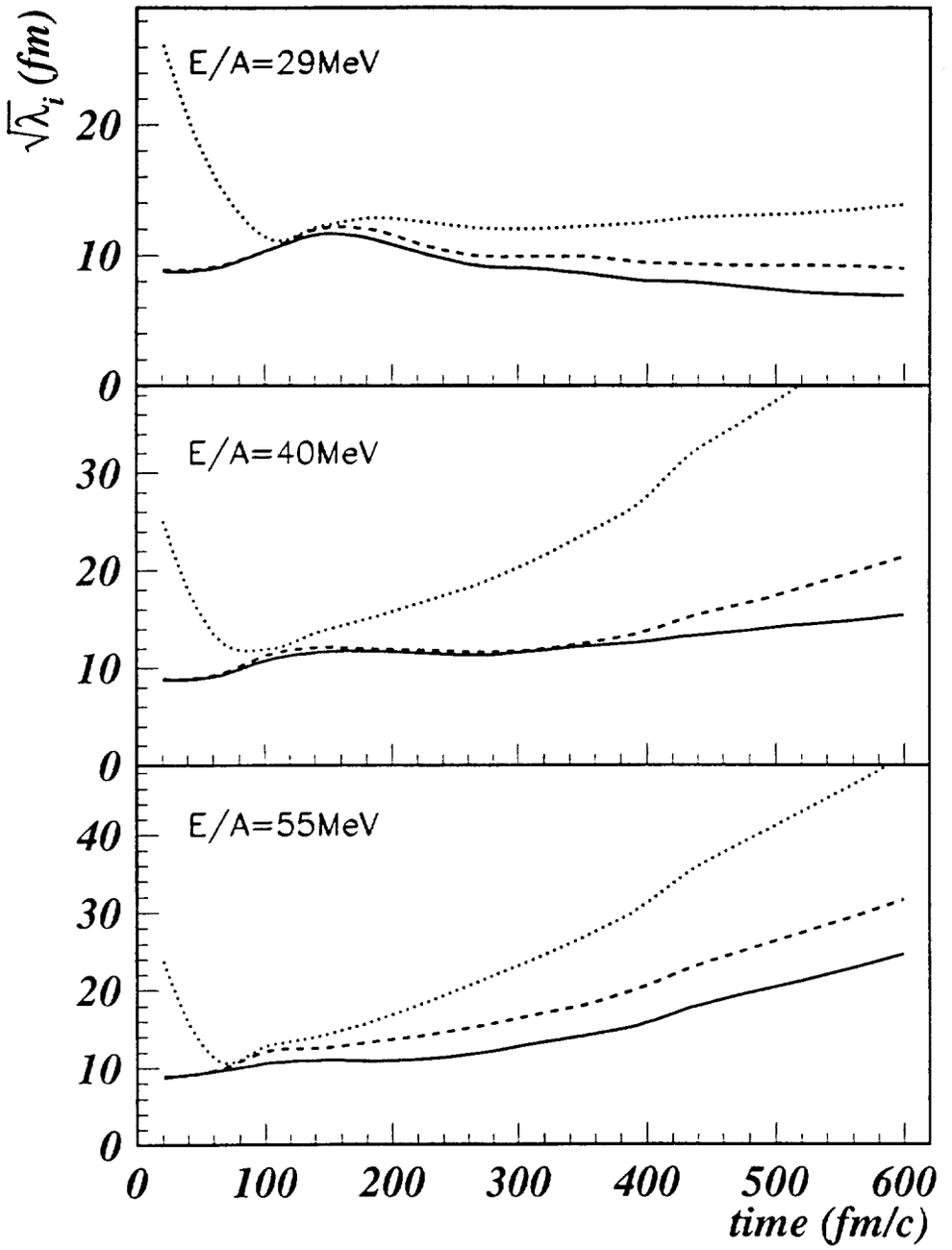
$\sqrt{\lambda_i}$ (fm)
E/A=29MeV
E/A=40MeV
E/A=55MeV
0
10
20
30
40
0
100
200
300
400
500
600
time (fm/c)

Figure 9